Resistive switching characteristics of Pt/CeO_x/TiN memory device

2014 Jpn. J. Appl. Phys. 53 060303

(http://iopscience.iop.org/1347-4065/53/6/060303)

Japanese Journal of Applied Physics **53**, 060303 (2014) **RAPID COMMUNICATION**
http://dx.doi.org/10.7567/JJAP.53.060303

Resistive switching characteristics of Pt/CeO_x/TiN memory device

Muhammad Ismail[1,3], Ijaz Talib[3], Chun-Yang Huang[1], Chung-Jung Hung[2], Tsung-Ling Tsai[1], Jheng-Hong Jieng[1], Umesh Chand[1], Chun-An Lin[1], Ejaz Ahmed[3], Anwar Manzoor Rana[3], Muhammad Younus Nadeem[3], and Tseung-Yuen Tseng[1*]

[1]*Department of Electronics Engineering and Institute of Electronics, National Chiao Tung University, Hsinchu 30010, Taiwan*
[2]*Department of Materials Science and Engineering, National Chiao Tung University, Hsinchu 30010, Taiwan*
[3]*Department of Physics, Bahauddin Zakariya University, Multan 60800, Pakistan*
E-mail: tseng@cc.nctu.edu.tw

Received February 18, 2014; accepted March 24, 2014; published online May 15, 2014

The resistive switching characteristics of Pt/CeO_x/TiN memory devices are investigated for potential applications in nonvolatile resistive random access memory (RRAM). The X-ray diffraction characteristics of the sputtered CeO_x layer indicate the formation of nanocrystalline single-phase CeO_2 with a cubic fluorite structure. The existence of oxygen vacancies in the Pt/CeO_x/TiN memory device was determined by X-ray photoelectron spectroscopic studies, while the presence of an interfacial layer between CeO_x and the TiN bottom electrode was investigated by X-ray diffraction and high resolution transmission electron microscopy. The TiON layer formed at the TiN/CeO_x interface seems to play a key role in the resistive switching mechanism of the device. The present CeO_x-based device shows excellent bipolar resistive switching characteristics, including a low operation current (100 μA), high ON/OFF resistance ratio (~10^5), and good retention/stress characteristics at both room temperature and 85 °C.

In recent years, resistive random access memory (RRAM) has attracted a great deal of attention from researchers. RRAM composed of a metal–insulator–metal (MIM) structure is being considered as a potential candidate to replace the flash memory in the near future. It demonstrates excellent characteristics including low power consumption, long data retention, high density integration, fast operational speed, high scalability, simple constituents, and low-cost nonvolatile memory applications.[1)] Many research groups have investigated RRAM using rare-earth materials[2–4)] and transition metal oxides.[5)] Rare-earth materials demonstrate very good resistive switching (RS) properties for nonvolatile memory. In addition, the transportation of oxygen vacancies/ions plays a key role in the resistive switching mechanism.[6)] Possessing a strong ability of oxygen ion/vacancy migration and good RS behavior, cerium oxide (CeO_2) thin films have gained a lot of interest for RRAM applications.[3,7)] Moreover, CeO_2 films present multivalent cations by exhibiting both +3 and +4 oxidation states and have high oxygen ion conductivity showing thir potential for valiancy change switching devices. In addition, the influence of the top/bottom electrode has been reported to enhance the window and stability for RS.[8)] Regarding the effect of the bottom electrode, it is shown that oxygen vacancies are generated due to the reaction between CeO_x and the TiN bottom layer.[9)] Consequently, an interfacial TiON layer is formed, which plays an important role in the RS behavior of the CeO_x/TiN memory device by working as an oxygen reservoir. The effect of Pt and Al as top electrodes on the RS behavior of CeO_2 films has also been studied.[3,10)] In fact, the set/reset voltage variability and progressive degradation of the RS devices are still severe challenges. The RS phenomena and conduction mechanisms involved in CeO_2-based devices are very important for RRAM applications. However, there is lack of systematic studies in various configurations using different electrode materials and discussing the mechanisms of the RS properties of CeO_x thin films.

In the present study, we report excellent bipolar resistive switching characteristics in the Pt/CeO_x/TiN memory devices with nonstoichiometric CeO_x films. The influence of TiN as a bottom electrode on the RS properties of CeO_x films and the switching mechanisms are also investigated.

First, a 100-nm-thick layer of a TiN bottom electrode (BE) was deposited on a SiO_2/Si substrate by an rf magnetron sputter employing a TiN target with a sputtering power of 100 W. Then, CeO_2 thin films (20–40 nm thick) were deposited on that TiN/SiO_2/Si substrate at room temperature by the same magnetron sputter using a ceramic CeO_2 target. A base pressure of 1.2×10^{-6} Torr was created in the chamber by a turbomolecular pump before deposition. The working pressure was maintained at 10 mTorr using a gas mixture of Ar and O_2 at a mixing ratio of 6 : 18 with a total flow rate of 20 sccm. The RF sputtering power of the system was set to 100 W. Finally, a 50-nm-thick Pt top electrode (TE) was deposited by dc magnetron sputtering on CeO_x/TiN/SiO_2/Si using a metal shadow mask with a diameter of 150 μm. The morphology and crystal structure were examined by high-resolution transmission electron microscopy (HRTEM) and X-ray diffraction (XRD), respectively. X-ray photoemission spectroscopy (XPS) analysis was performed to identify the composition of the CeO_x film in the device. The thickness of different layers were confirmed by HRTEM. The electrical characteristics of the device were measured using a semiconductor parameter analyzer (Agilent B1500A) at room temperature. During electrical measurements, a bias voltage was applied to Pt TE keeping the TiN BE grounded.

The XRD pattern of the Pt/CeO_x/TiN memory device shown in Fig. 1(a) indicates the formation of a single-phase polycrystalline CeO_2 showing a cubic fluorite structure. From the broadness and weak intensity of diffraction peaks, the poor crystalline structure can be inferred and defects such as oxygen vacancies may be anticipated in the film matrix. Moreover, few weak reflections corresponding to the TiON monoclinic structure are also observed as marked in Fig. 1(a). Figure 1(b) illustrates a cross-sectional TEM image of the Pt/CeO_x/TiN/SiO_2/Si RRAM device demonstrating an apparent interface between CeO_x and the TiN bottom electrode. Regarding the chemical surface composition and the valence/oxidation state of various species, Fig. 2(a) displays the Ce 3d XPS spectrum of CeO_x films along with their corresponding deconvoluted plots. The XPS peaks

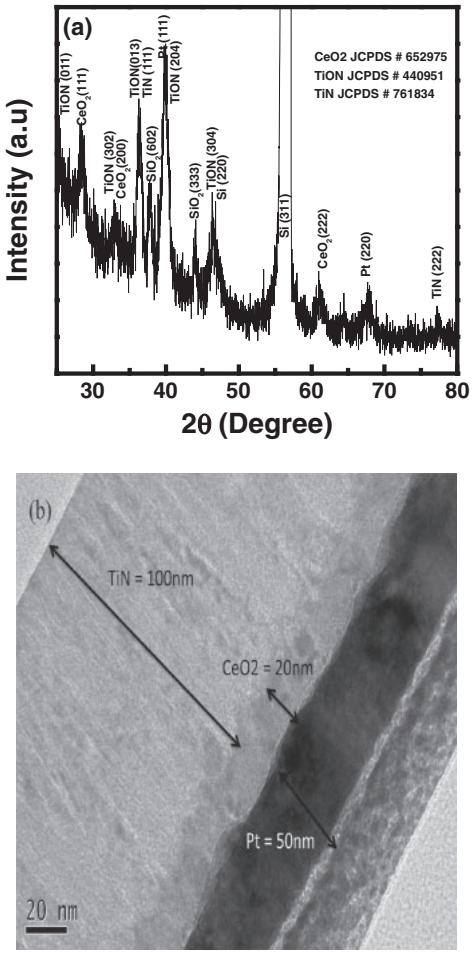

Fig. 1. (a) XRD pattern of Pt/CeO_2/TiN/SiO_2/Si structure. (b) HRTEM cross-sectional image of Pt/CeO_2/TiN/SiO_2/Si device.

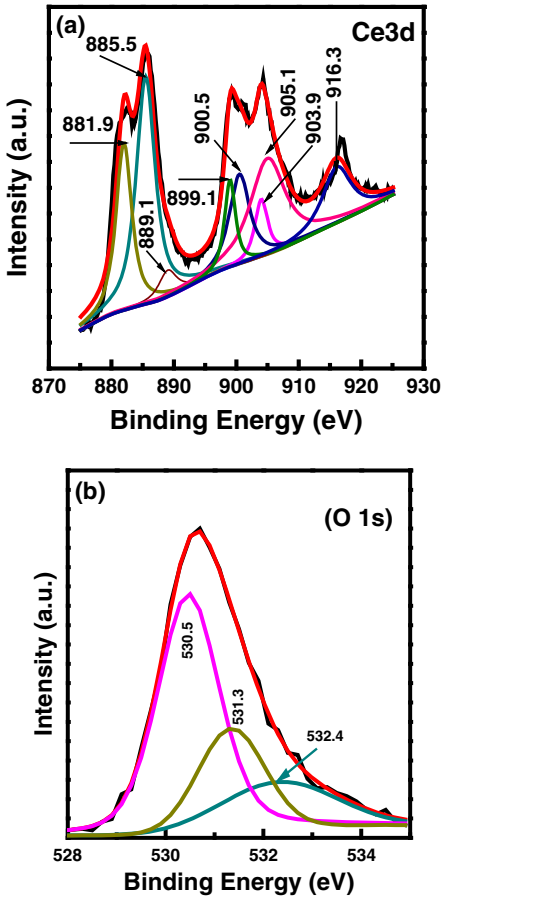

Fig. 2. (Color online) XPS core level spectra of CeO_2 film (a) Ce 3d level and (b) O 1s level.

located at 881.9, 885.5, and 889.1 eV correspond to Ce $3d_{5/2}$, while peaks at 899.1, 900.5, 903.9, 905.1, and 916.3 eV are attributed to Ce $3d_{3/2}$. The XPS features at 885.5 and 903.9 eV are the characteristic peaks of Ce^{3+}, and the peak at 916.3 eV corresponds to the initial electronic state of the Ce^{4+} ion.[11,12] This implies that both Ce^{4+} and Ce^{3+} ions coexist as Ce^{4+}/Ce^{3+} pairs in the CeO_x layer. The concentrations of Ce^{4+} and Ce^{3+} as obtained from the deconvoluted XPS spectra are 39.6 and 60.4%, respectively. A higher percentage of Ce^{3+} ions indicates the richness of oxygen vacancies.[13] It is reported that Ce^{3+} ions distribute themselves around oxygen vacancies in CeO_2 and their presence would enhance the local electronic conductivity of the oxide.[14] Under an external bias, if the field of Ce^{3+} ions bridges the top and bottom electrodes, conductive paths would be formed to switch the device from high resistance state (HRS) to low resistance state (LRS). Figure 2(b) shows the O 1s XPS spectrum of the Pt/CeO_x/TiN device consisting of three peaks at binding energies of 530.5, 531.3 and 532.4 eV, which can be attributed to lattice oxygen,[15] oxygen vacancies,[16] and oxygen ions[12] in CeO_2 respectively. Furthermore, Holgado et al.[17] have shown that the removal of oxygen during sputtering may lead to the formation of Ce^{3+} ions, which causes the development of a new peak in the O 1s spectrum at a binding energy of 532.4 eV and they attributed the peak to oxygen ions at the surface (and grain boundaries) of the film.

Figure 3(a) depicts the current vs bias voltage sweep characteristics demonstrated for CeO_x films with varying thickness in the range of 20–40 nm indicating the negative SET and positive RESET typical for bipolar RS memory. Initially, by sweeping the bias voltage from 0 to −3 V, a sudden increase in the current of all three devices is observed with a current compliance of 1 mA switching them to a LRS. A notable point is the magnitude of the negative bias voltage needed to switch the device from HRS to LRS, which increases with a rise in thickness of the sandwiched CeO_x film. Such a dependence of V_{set} upon the thickness of the CeO_x films signifies that the SET process is a field-induced phenomenon. However, the bias voltage needed for the subsequent RESET process is not evidently affected by the thickness of the CeO_x film. Consequently, the electric power needed for the rupture of conductive filaments is the same for all three devices. Typical forming free bipolar resistive switching characteristics of a Pt/CeO_x/TiN RRAM memory device are displayed in Fig. 3(b). Figure 3(b) that the fresh device is originally in the high resistance state and the negative SET voltage of the 1st sweep is almost the same as those of the 100th and 200th sweeps in contrast to the devices which need a large (forming) voltage for their first SET process. As far as power consumption in the device preparation for repeatable resistive switching is concerned, such forming free resistive switching behavior is very promising from an RRAM application point of view.[2,18]

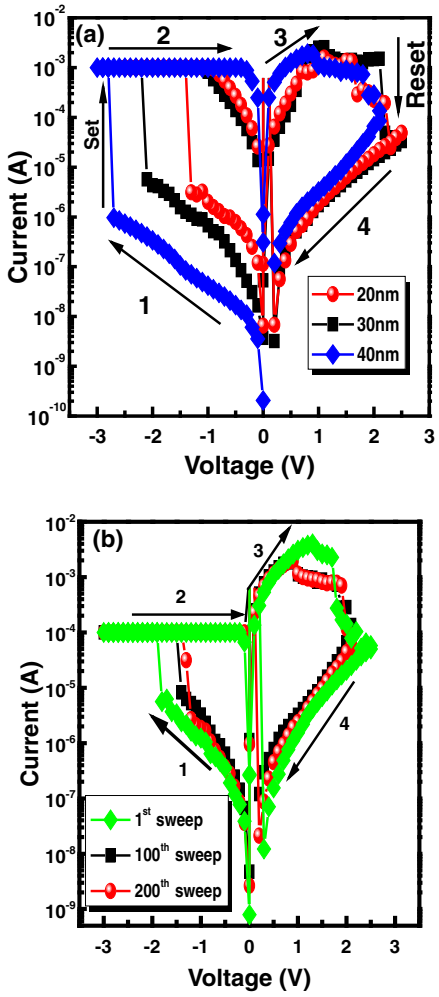

Fig. 3. (Color online) (a) Current–voltage (I–V) characteristics as a function of CeO_2 film thickness that varies from 20 to 40 nm in Pt/CeO_x/TiN RRAM memory devices. (b) DC I–V cycling characteristics studied at V_{read} of 0.3 V over 200 sweeps for 30-nm-thick CeO_2 memory device.

To further evaluate the memory performance of the Pt/CeO_x/TiN device, an endurance test is conducted at room temperature and 85 °C, as shown in Fig. 4. The resistances were determined at a fixed voltage of 0.3 V, while the set and reset operations were performed at negative and positive voltage polarities, respectively. The HRS resistance measured at 85 °C was lower than that at room temperature. The high resistance can be described as exhibiting a typical semiconductor-like behavior,[19] with the resistance decreasing by approximately 2 orders of magnitude upon increasing the temperature. However, the LRS resistance at 85 °C was slightly lower than that at RT, indicating once again the semiconducting behavior. The resistance ratio of HRS to LRS lies approximately in the range of 10^3–10^5 during the first 200 cycles. After 200 switching cycles, it can be seen that the device still has an acceptable memory window, demonstrating its good repetitive switching capability. On comparing the results with a work[9] on a similar Pt/CeO_x/TiN memory device, it can be concluded that our device exhibits a larger memory window for read/write operations with low power consumption and a much better repetitive switching capability. This may be attributed to the different conditions of the oxide film in the ReRAM device.

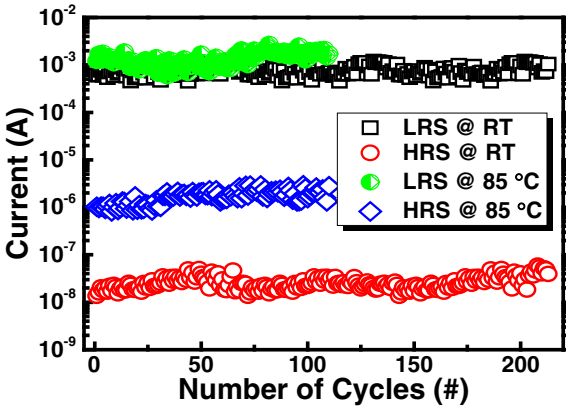

Fig. 4. (Color online) Endurance characteristics of Pt/CeO_x/TiN device measured at RT and 85 °C.

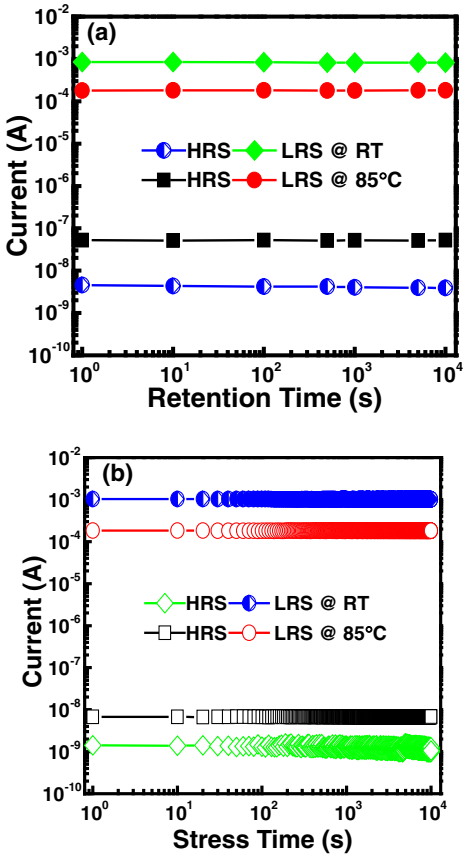

Fig. 5. (Color online) (a) Retention characteristics of HRS and LHS of Pt/CeO_x/TiN device under a continuous reading voltage of 0.3 V. (b) Non-destructive readout properties of both ON- and OFF-states at RT and 85 °C.

Figure 5(a) shows the retention performance of both HRS and LRS for the Pt/CeO_x/TiN device. It is evident that the device retains its ON/OFF state for more than 10^4 s without any apparent degradation at both room temperature and 85 °C. As shown in Fig. 5(b), the two resistance states are stable over 10^4 s under a stress voltage of 0.3 V, without any observable degradation at both room temperature and 85 °C, demonstrating excellent nondestructive readout capability. Such superior data retention characteristics of the Pt/CeO_x/TiN device reveal its potential for future nanoscale nonvolatile memory applications.

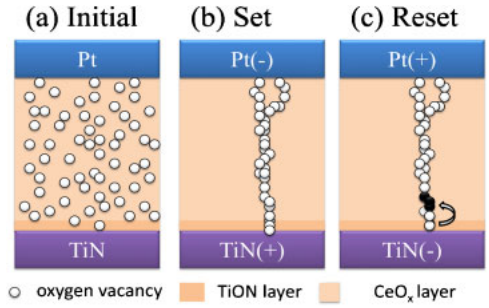

Fig. 6. (Color online) Schematic diagram of resistive memory switching mechanism in Pt/CeO_x/TiN memory device. (a) Initial state, (b) set to LRS and (c) reset back to HRS. Black circles indicate the rupture area of the device during the reset process.

Figure 6 presents a schematic description about of the resistive switching mechanism of the device. In the pristine state, a large number of oxygen vacancies exist in the CeO_x layer (Fig. 2). However, as these oxygen vacancies are randomly distributed and are not yet arranged to form conductive filaments, the device is initially in HRS, as shown in Fig. 6(a). During the SET transition, when a negative bias voltage is applied to Pt TE, oxygen ions migrate from the CeO_x layer to the bottom electrode and oxygen vacancies drift under the applied field to form the conductive filaments, and thus switch the device into LRS, as shown in Fig. 6(b). It is notable that the filamentary path starts to develop from the oxygen-deficient interfacial TiON layer near the BE. This interfacial TiON layer is formed due to the oxygen gettering property of TiN (which can take oxygen from the CeO_x layer to form a partially oxidized TiON layer[9]). The enhanced oxygen mobility facilitates the reduction of Ce^{4+} cations, and creates more Ce^{3+} and oxygen vacancies (Fig. 2). In contrast, the positive bias applied to the Pt top electrode attracts the oxygen ions from the TiON layer to drift back to the CeO_x film thereby oxidizing the vacancies, hence rupturing the formed conductive path and resulting in a transition from LRS to HRS, as shown in Fig. 6(c). In this case, the TiON layer might be the source of mobile oxygen. The TiN BE thus works as an oxygen ion reservoir, which causes the migration of oxygen ions under an external bias hence contributing significantly to the resistance change.[8,20,21]

Bipolar RS characteristics were successfully demonstrated in a Pt/CeO_x/TiN device. The XRD pattern of a magnetron-sputtered CeO_x layer indicated the formation of a single-phase CeO_2 with a cubic polycrystalline fluorite structure. The presence of oxygen vacancies was determined by XPS spectra while the presence of an interfacial layer between CeO_2 and TiN was detected from the HRTEM image. The set voltage dependence on the thickness of the CeO_x layer has indicated that the switching process is an electric-field-induced phenomenon. The TiN/CeO_x interface plays a key role in controlling the oxygen vacancy defects, which in turn control the formation/rupture of conducting filaments composed of oxygen vacancies. The device exhibited a good cycling endurance with a large memory window (ratio of HRS/LRS about 10^5) and an acceptable retention/stress test for 10^4 s. The cycling endurance and data retention capability of the device were found to be satisfactory at 85 °C.

Acknowledgements The authors acknowledge the financial support by the Higher Education Commission (HEC), Islamabad, Pakistan under the International Research Support Initiative Program (IRSIP). This work was also supported by the National Science Council, Taiwan, under project NSC NSC 99-2221-E009-166-MY3.

1) T. Y. Tseng and S. M. Sze, *Nonvolatile Memories: Materials, Devices and Applications* (American Scientific Publishers, Stevenson Ranch, CA, 2012) Vol. 2, Chaps. 5–14.
2) D. Panda and T. Y. Tseng, Thin Solid Films **531**, 1 (2013).
3) C.-Y. Lin, D.-Y. Lee, S.-Y. Wang, C.-C. Lin, and T.-Y. Tseng, Surf. Coatings Technol. **203**, 480 (2008).
4) K. C. Liu, W. H. Tzeng, K. M. Chang, Y. C. Chan, C. C. Kuo, and C. W. Cheng, Microelectron. Reliab. **50**, 670 (2010).
5) T. M. Pan and C. H. Lu, Appl. Phys. Lett. **99**, 113509 (2011).
6) S.-Y. Wang and T.-Y. Tseng, J. Adv. Dielectr. **1**, 141 (2011).
7) X. Cao, X. Li, X. Gao, W. Yu, X. Liu, Y. Zhang, L. Chen, and X. Cheng, J. Appl. Phys. **106**, 073723 (2009).
8) C. Y. Lin, C. Y. Wu, T. C. Lee, F. L. Yang, C. Hu, and T. Y. Tseng, IEEE Electron Device Lett. **28**, 366 (2007).
9) Q. Zhou and J. Zhai, Integrated Ferroelectr. **140**, 16 (2012).
10) X. Sun, B. Sun, L. Liu, N. Xu, X. Liu, R. Han, J. Kang, G. Xiong, and T. P. Ma, IEEE Electron Device Lett. **30**, 334 (2009).
11) E. Bêche, P. Charvin, D. Perarnau, S. Abanades, and G. Flamant, Surf. Interface Anal. **40**, 264 (2008).
12) M. Ismail, C. Y. Huang, D. Panda, C. J. Hung, T. L. Tasi, J. H. Jeing, C. A. Lin, U. Chand, A. M. Rana, E. Ahmed, I. Talib, M. Y. Nadeem, and T. Y. Tseng, Nanoscale Res. Lett. **9**, 45 (2014).
13) F. Meng, C. Zhang, Q. Bo, and Q. Zhang, Mater. Lett. **99**, 5 (2013).
14) S. Deshpande, S. Patil, S. Kuchibhatla, and S. Seal, Appl. Phys. Lett. **87**, 133113 (2005).
15) R. Yu, L. Yan, P. Zheng, J. Chen, and X. R. Xing, J. Phys. Chem. C **112**, 19896 (2008).
16) D. Gao, G. Yang, L. Li, J. Zhang, J. Zhang, and D. Xue, J. Phys. Chem. C **114**, 18347 (2010).
17) J. P. Holgado, G. Munuera, J. P. Espinós, and A. R. González-Elipe, Appl. Surf. Sci. **158**, 164 (2000).
18) C. Chen, Y. C. Yang, F. Zeng, and F. Pan, Appl. Phys. Lett. **97**, 083502 (2010).
19) J. L. Her, T. M. Pan, and C. H. Lu, Thin Solid Films **520**, 5706 (2012).
20) J. Kim, K. Lee, Y. Kim, H. Na, D.-H. Ko, H. Sohn, and S. Lee, Mater. Chem. Phys. **142**, 608 (2013).
21) M. Fujimoto, H. Koyama, M. Konagai, Y. Hosoi, K. Ishihara, S. Ohnishi, and N. Awaya, Appl. Phys. Lett. **89**, 223509 (2006).